WAVEFRONT SENSING: FROM HISTORICAL ROOTS TO THE STATE-OF-THE-ART

H.I. Campbell[1] and A.H. Greenaway[1]

Abstract. This paper provides an overview of wavefront sensing technologies. A brief background to the field of wavefront sensing is given, and several wavefront sensors are studied in detail. Particular attention is given to the Shack-Hartmann, Phase Diversity and Curvature wavefront sensors. Interferometric and Pyramid wavefront sensors are discussed as well as Schlieren imaging, algorithmic approaches (such as image sharpening), Shack-Hartmann Curvature hybrid wavefront sensing and modal wavefront sensors.

1 Introduction

Since the birth of modern Adaptive Optics (AO) in 1953 (Babcock) wavefront sensors have played an important role in the design of AO systems. Wavefront sensing provides the means to measure the shape of an optical wavefront or, in the case of a closed-loop AO system, the deviation of the wavefront from the diffraction-limited case (Greenaway & Burnett 2004). Depending on the design, wavefront sensors may be used either to generate a signal related to the wavefront deformation, or to provide a full reconstruction of the wavefront shape. In the closed-loop case one seeks to minimise the error signal through manipulation of the wavefront by a corrective element. Full reconstruction of the wavefront is more time consuming, but is sometimes necessary. In metrology applications the shape of the wavefront may represent the shape of a physical surface under test.

The phase/Optical Path Difference (OPD) of a wavefront can be measured directly in a number of ways, which can include; Interferometric methods (Tyson 1991), Fraunhoffer diffraction patterns (Gonsalves 1987b), moments of diffraction, multiple intensity measurements (Gonsalves 1987b; Robinson 1978) or in exceptional cases from a single intensity measurement and the use of *a priori* information (Dainty & Fiddy 1984). This information can then be fed back to the corrective

---

[1] School of Engineering and Physical Sciences, Heriot-Watt University, Edinburgh EH14 4AS, UK; e-mail: `a.h.greenaway@hw.ac.uk`

element. Phase cannot be measured directly, there can be problems with these methods determining the uniqueness of the solution and they often only apply to small angles, *i.e.* wavefronts which are not greatly aberrated (Burge *et al.* 1976; Barakat & Newsam 1984; Carmody *et al.* 2002). The indirect approach to wavefront sensing is to compensate for the wavefront error without explicitly calculating the full wavefront reconstruction. The Multi-Dither technique is perhaps the most well known example of an indirect wavefront sensing system (Youbin *et al.* 1998).

In Zonal sensors the wavefront is expressed in terms of the OPD across a small spatial area, for example a subaperture. If the wavefront is subdivided by N subapertures, then as $N \to \infty$ the wavefront is fully represented. If wavefront tilts are measured across the subapertures they can be integrated to provide the full wavefront shape. The Shack-Hartmann wavefront sensor is the most commonly used zonal sensor and will be covered in detail later. In Modal sensors the wavefront is described by decomposition into a set of orthogonal polynomials (Tyson 1991; Gureyev *et al.* 1995, 1996; Neil *et al.* 2000). The most common basis set for these sensors is Zernike Polynomials which have the convenient property of forming an orthonormal set across circular apertures (Noll 1976). Curvature sensing and Phase Diversity (PD) are both examples of modal wavefront sensing and are also discussed in some depth in later sections. Tyson (1991) proposes that as a general rule, if low order aberrations dominate it is best to use modal wavefront sensing, whereas when higher order aberrations are involved zonal methods will give better performance. For AO in the presence of the atmosphere it is often useful to use a combination of both, employing a zonal method to correct for tilt errors and a modal method to reconstruct the wavefront in terms of Zernike polynomials.

However, for the correct choice of wavefront sensor, practical issues such as hardware limitations, the speed required, computational power available and ease of integration into the existing optical system must be considered. In this paper, we will consider a number of different wavefront sensors from historically important techniques to the sensors in common use today.

2   The Shack-Hartmann Wavefront Sensor

The Shack-Hartmann (S-H) wavefront sensor is the most well known and widely used wavefront sensor today. It was developed in 1971 by Roland Shack and Ben Platt (Platt & Shack 2001) in response to the US Air Force's need to improve images of satellites taken from the Earth, which were distorted by the Earth's atmosphere. The S-H sensor is an adaptation of the earlier Hartmann plate method of wavefront sensing (Greenaway & Burnett 2004) and was altered to be more efficient for low-light applications like astronomy.

The S-H is a zonal wavefront sensor which provides a measurement of the local first derivative (slope) of the input wavefront. This is achieved by dividing the wavefront using an array of lenslets, each taking a portion of the beam and focusing it onto a detector array. This use of lenslets was the main innovation on the Hartmann plate design which used an array of holes to separate the wavefront into pencil-like beams. The added light gathering efficiency of the lenslets made
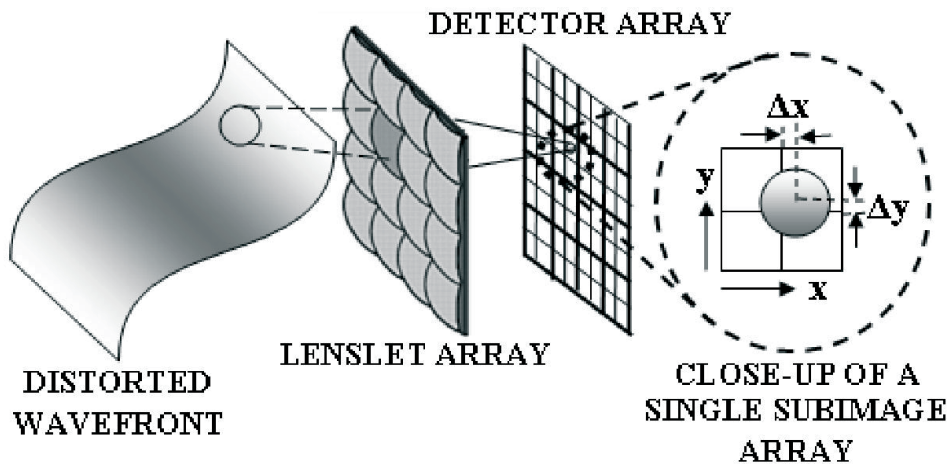
Fig. 1. Schematic of the basic Shack-Hartmann Wavefront Sensor.

the new S-H sensor ideal for photon-starved situations like astronomy (Platt & Shack 2001). Figure 1 shows the basic architecture of the S-H sensor.

The detector array is arranged such that a sub-array of pixels is assigned to each subaperture image. In Figure 1 this is shown as a simple quad-cell for each lenslet, although more pixels can be used depending on the size of the detector and the number of lenslets. When a plane wave is incident on the lenslet array a tightly focussed spot will appear in the centre of each sub-area of the detector (corresponding to the optics axis of the particular lenslet). When the input wavefront is distorted the sub-images will be shifted in the x and y directions (demonstrated in the close-up in Fig. 1). The centroid of each image can be used to calculate the slope of the wavefront across its associated subaperture. The wavefront is reconstructed by combining the local slope measurements across the lenslet array. Depending on the type of aberration present in the input wavefront the shape of the sub-images will also be distorted. Since the slope of the wavefront does not depend on the wavelength, the S-H is an achromatic wavefront sensor. Figure 2 shows examples of simulated Hartmann spot patterns generated by a perfect human eye, and an aberrated one (Williams 2005).

The advantages of the S-H sensor are its wide dynamic range, high optical efficiency, white light capability, and ability to use continuous or pulsed sources (Tyson 1991). The sensitivity and accuracy of the S-H sensor are excellent across the wide dynamic range of the instrument. This makes it a very attractive device where large dynamic ranges are required. As the wavefront aberration increases the sub-images are displaced further from their local optic axis, the dynamic range is limited to aberrations which do not allow the sub-images be displaced outwith their own sub-array. Therefore the range is largely limited by the size of the detector array. The S-H sensor can also be used to study the intensity and phase
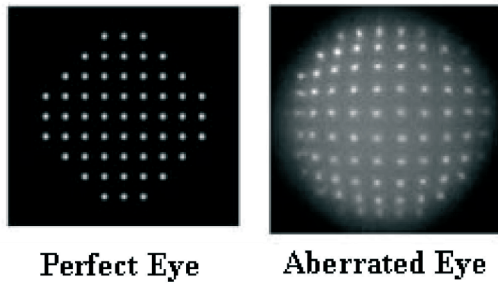
Fig. 2. Example Hartmann spot patterns for perfect and aberrated eyes (Williams 2005). Used courtesy of David Williams' Laboratory, University of Rochester.

information simultaneously by measurement of the spot amplitude and position respectively (Levecq 2005). One drawback is the precision required in alignment and calibration of this device. Vibration or distortion of the optics could lead to shifts in the spot positions, which in turn would give incorrect measurements of the wavefront slope. There are numerous variations on the basic S-H design to attempt to minimise alignment and calibration problems (Rousset *et al.* 1993). A second disadvantage is that this type of wavefront sensor is not well suited to dealing with extended sources. When the object being imaged is large then the shape of the object will be convolved with the diffraction pattern of the subaperture, and optical cross-correlation is required to remove this effect. This takes a lot of computational effort and time (Rao *et al.* 2002; Welch *et al.* 2003). Finally, the number of pixels required in the detector to create one phase data point is much higher than in curvature sensors (Levecq 2005). For high spatial resolutions large CCD cameras are required and this can be expensive and adds extra weight to the optical system.

The S-H sensor's white light capability and optical efficiency make it a favourite among astronomers. Also, since astronomy applications mainly involve point sources, the problems encountered with extended sources are less of an issue. This wavefront sensor has also been used extensively in ophthalmic applications. Since the first paper published by Dreher *et al.* (1989) many researchers have chosen this sensor for use in improving retinal imaging and mapping the aberrations of the eye (Liang *et al.* 1994; Hofer *et al.* 2001; Shahidi *et al.* 2004). It is also highly suitable for laser testing, and in AO systems (Platt & Shack 2001; Kudryashov *et al.* 2003).

## 3   Phase Diversity and Curvature Wavefront Sensing

Phase Diversity (PD) is a phase retrieval algorithm which measures the wavefront phase through intensity images (Gonsalves 1982, 1987a, 1987b; Jeffries *et al.* 2002). Gonsalves (1982) first proposed PD as one of a new class of algorithms
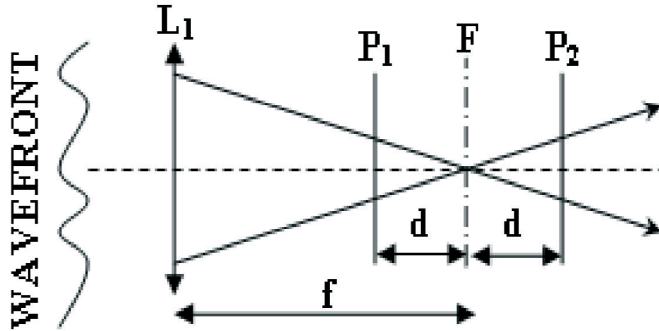
Fig. 3. A Schematic of the Curvature Sensing scheme (Roddier 1988). Intensity images are obtained on planes P_1 and P_2 symmetrically about the focal plane F.

designed to ensure the uniqueness of the computed phase solution (Schiske 1975; Teague 1982). It is not possible in general to obtain a unique solution from a single intensity image, instead multiple images or *a priori* information must be used to calculate the correct solution (Greenaway & Burnett 2004; ESO website 2003). Where multiple images are used these should be captured on a time-scale short in comparison to any phase changes. The name "Phase Diversity" refers to the fact that both images contain a deliberately added (and therefore known) phase term, in addition to the unknown wavefront phase. The wavefront phase can be calculated from the phase diverse intensity images using iterative algorithms. Many such algorithms have been proposed over the years, from versions of the Gerchberg-Saxton (Gerchberg & Saxton 1972) to more complicated approaches such as genetic algorithms (Thust *et al.* 1997; Carmody *et al.* 2002; Give'on *et al.* 2003), simulated annealing (Thust *et al.* 1997; Nieto-Vesperinas *et al.* 1988) and neural networks (Kendrick *et al.* 1994). These solutions are computationally expensive and the time taken to calculate the solution has, in the past, meant that this type of wavefront sensor is not fast enough for real-time AO applications. Curvature Sensing and Generalised Phase Diversity, which will both be discussed later, are variations of the PD method which do not suffer from the same speed limitations as classic PD algorithms.

Roddier first introduced the Curvature Sensor (CS) in 1988, a special class of PD wavefront sensor which measures the local wavefront curvature using a pair of intensity images with equal and opposite aberration, captured symmetrically about either the image or pupil plane of the optical system (shown in Fig. 3). The wavefront curvature is mathematically related to the difference of these intensity images by the Intensity Transport Equation (ITE). There exist a great number of algorithms to solve this equation and retrieve the wavefront phase through its curvature (Teague 1983; Gureyev *et al.* 1995, 1996; Quiroga *et al.* 2001; van Dam & Lane 2002, 2002; Woods & Greenaway 2003).
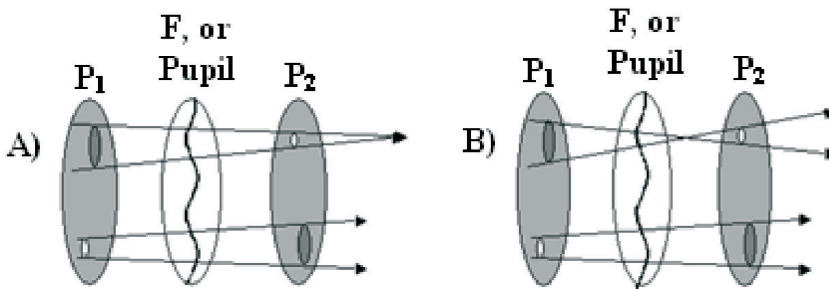
Fig. 4. A) Schematic showing the relationship between intensity images (formed on planes P_1 and P_2) and wavefront curvature (in the focal, F, or pupil plane). **B)** Shows the ambiguity caused by a focus between the two planes.

Figure 3 is an example CS system. An input wavefront is focussed by a lens or mirror (labelled L_1), and a pair of intensity images are captured symmetrically about the focal plane (at planes P_1 and P_2). This may be achieved in a number of ways including physical displacement of the image plane (Barty *et al.* 1998), use of vibrating mirrors (Roddier 1988), or by beam-splitters and folded paths.

Figure 4A demonstrates how the intensity in the 2 recording planes can be related to the local curvature of the wavefront. Portions of the wavefront which are locally concave will converge as they propagate to form a smaller, brighter, patch at the corresponding position on P_2 than was seen on P_1. The opposite is true of portions of the wavefront which are convex. The difference of the two intensity images provides an approximation of the axial intensity gradient between the image planes. This approximation will hold if the wavefront curvature is not too strong. If a focal point occurs within the volume (as shown in Fig. 4B) an ambiguity arises as it is impossible to know whether light at P_2 is coming from a focus, or from a convex portion of the wavefront. The maximum allowable distance between the planes will therefore depend on the strength of the wavefront curvature. A highly aberrated wavefront will have greater curvature, therefore concave portions of it will focus strongly and thus the distance between the sampling planes must be kept small to avoid ambiguity. This limits the dynamic range of the system.

In Phase Diversity (PD) a pair of intensity images is obtained by adding different amounts of diversity phase (defocus) to the unknown wavefront. This pair could be the in-focus image and one phase-diverse image, or two phase-diverse images. In most cases the diversity phase added is defocus as it may be easily applied by a number of methods, one of which is demonstrated in Figure 5. Images recorded symmetrically placed about focus (as shown in Fig. 3) will contain equal and opposite amounts of defocus. In this case PD and CS are essentially the same technique and the wavefront phase is obtained by solution of the ITE. Where CS and PD differ is when the diversity phase used is not defocus, when
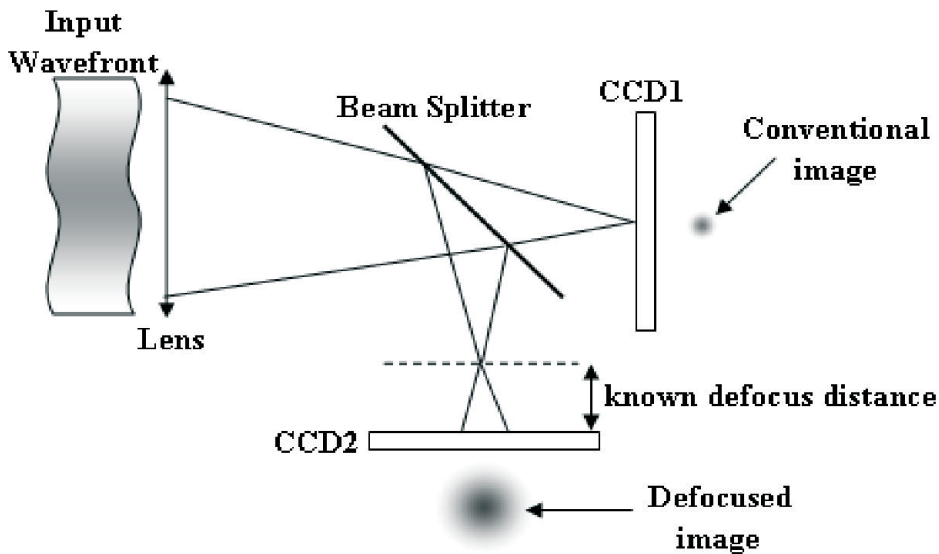
Fig. 5. An example of a Phase Diversity system. A pair of intensity images are obtained on the CCD cameras, one is the in-focus image and the other is defocused by a known amount.

the phase-diverse images do not contain equal and opposite amounts of defocus, or are not obtained symmetrically about the focus or pupil plane of the system.

As previously discussed there are several means of obtaining the pair of intensity images for CS and defocus-only phase diversity (DPD). When using these techniques DPD and CS are suitable for use with white-light or broadband sources. Another method of applying the phase diversity, using a diffraction grating, has been proposed (Blanchard & Greenaway 1999, 2000a, 2000b; Blanchard *et al.* 2000). The grating, essentially an off-axis Fresnel zone plate, has a different effective focal length in each diffraction order. Combining the grating with a lens, and keeping the image distance constant, in each diffraction order a different object plane will be imaged; this is demonstrated in Figure 6. The difference between the intensity images in the ± 1 orders may then be used in the ITE to solve for the wavefront phase. This diffraction grating based wavefront sensor is light-weight, robust, and due to its common-path design is very compact. It also does not suffer from the alignment problems of the Shack-Hartmann lenslet arrays. Use of a single grating does limit the wavefront sensor to a narrow wavelength band and an appropriate filter must be used with broadband sources. This could potentially be a problem in photon-starved applications like astronomy, but in metrology it is possible to simply use a higher power source. Blanchard & Greenaway (2000a) have described how this technique can be extended to broadband sources using a pair of blazed gratings to provide dispersion and create a beam offset proportional to
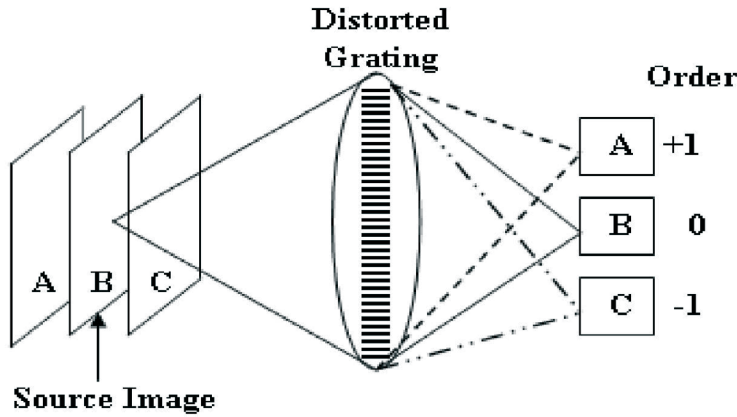
Fig. 6. Schematic of the diffraction grating based Defocus only Phase Diversity Sensor. This diagram demonstrates the simultaneous multi-plane imaging operation of this sensor

wavelength whilst leaving the relative propagation distance of each wavelength the same. This reduces the chromatic blurring of the phase diverse intensity images and allows the grating based DPD sensor to be used in true colour applications like retinal imaging.

3.1 Generalised Phase Diversity

In his original 1982 paper Gonsalves suggested that defocus may not be the best phase diversity to add in all cases. There is a growing interest in the use of other diversity functions in the hopes of building ever more sensitive wavefront sensors (Greenaway *et al.* 2003; Campbell *et al.* 2004a; Dolne & Schall 2004; Smith 2004; Smith & Wick 2004). Generalised Phase Diversity (GPD) is a new form of PD wavefront sensor that is not limited to, but may include, the use of defocus as the diversity phase (Greenaway *et al.* 2003; Zhang *et al.* 2003; Campbell *et al.* 2004a, 2004b, 2005). The GPD sensor can exploit the diffraction grating based principle shown above (Blanchard & Greenaway 1999, 2000a, 2000b; Blanchard *et al.* 2000), except that the diffraction grating is now programmed with a diversity function which may not be defocus. The symmetry conditions the diversity function must meet to be suitable for use in a null wavefront sensor are outlined by Campbell *et al.* (2004a). It is anticipated that this new wavefront sensor will be better suited for use with discontinuous and scintillated wavefronts than the DPD sensor, by avoiding the limiting assumptions necessary for solving the ITE and instead employing a new analytical solution for the wavefront phase (Campbell *et al.* 2005; Zhang *et al.* 2005).

GPD creates phase diverse data through the convolution of the input wavefront with a blur function, which is chosen and programmed into the grating. This convolution process is similar to the concept of wavefront shearing (which

is discussed in Sect. 5) since the wavefront interferes with itself over local regions determined by the spatial extent of the blur function. This leads to the interesting property that the wavefront phase change need only be small across the width of the blur function, the overall peak-to-valley (PV) aberration can be relatively large (Campbell *et al.* 2005; Zhang *et al.* 2005). This can be exploited to improve the dynamic range and will allow the GPD sensor to be used in a wide variety of applications where large wavefront errors are expected.

Since Gonsalves first proposed that diversity functions other than defocus may have advantages in particular applications results have been published demonstrating superior results obtained using Spherical Aberration (Campbell *et al.* 2004a, 2004b), and Astigmatism (Dolne & Schall 2004). This is an area of PD wavefront sensing which is of increased interest and may allow PD to be tailored to maximise sensitivity in particular applications.

3.2   *Phase Diversity and Curvature Sensor – Advantages and Disadvantages*

In comparison to the Shack-Hartmann, CS and PD wavefront sensors offer several important advantages. The first is that, since curvature is a scalar field it only requires one value per point. This means there is a reduction in the number of detector pixels required to measure the wavefront, and thus a saving in both cost and overall size. Secondly, curvature measurements are more efficient than tilt measurements, which are highly correlated (Roddier 1988). This makes CS and PD better suited for use with extended sources. It is also possible with these sensors to use the signal they generate to directly drive a corrective element (such as a bimorph or membrane mirror (Roddier 1988). This is much faster, and less computationally expensive, than performing a full reconstruction when it is not strictly needed.

4   The Paterson-Dainty Hybrid Sensor

In 2000, Paterson and Dainty published their first results with a hybrid wavefront sensor which combines the Shack-Hartmann and Curvature Sensors (Paterson & Dainty 2000). The configuration of the Hybrid Sensor (HS) is similar to the Shack-Hartmann (see Fig. 1), the principle difference being the use of astigmatic lenslets to form the lenslet array. The idea is based on the astigmatic focus sensor of Cohen *et al.* (1984), which measures wavefront curvature using the shape and position of the wavefront's image through an astigmatic lens. The image is detected by a quad-cell detector (see Fig. 1), when the wavefront is un-aberrated the image will be circular and on axis. If defocus is present in the beam then the image will be elliptical and oriented at 45° to the axis. Therefore, in the HS the shape of each intensity sub-image can be used to measure the local wavefront curvature at that lenslet. The sensor response to the input wavefront aberration will depend on the astigmatic parameters of the lenslet, the quad-cell dimensions and the geometry of the lenslet array (Paterson & Dainty 2000).
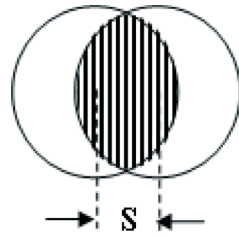
Fig. 7. A demonstration of lateral shear S between two beams. Interference can only occur where the beams overlap.

The HS has a limited range over which the defocus and the curvature signal are linearly related, but this range is large enough for closed-loop AO operation (Paterson & Dainty 2000). Paterson and Dainty's results have shown that the HS is most sensitive to defocus and spherical aberration. While the Shack-Hartmann (gradient-only) sensor has a wide range of mode sensitivities (and is more sensitive to some modes than others) and Curvature sensors have almost equal sensitivities to all modes, the HS was proven to have improved modal sensitivity compared to either sensor on its own. This is the main advantage of the HS, that whilst retaining the simple design of the Shack-Hartmann, it has increased modal sensitivity. This may mean that in an AO system the Hybrid Sensor would allow more modes to be properly corrected (Paterson & Dainty 2000).

5   Wavefront Shearing Interferometry

Wavefront Shearing Interferometry (WSI), like the Shack-Hartmann, is a wavefront sensing method that can be used to measure the slope of the wavefront. In the 1970's and 1980's the WSI was very much in vogue as a means of reconstructing the input wavefront (Roddier 1976; Greenaway & Roddier 1980; Roddier & Roddier 1986), and found application particularly in the correction of atmospheric distortions on astronomical images, measurement of stellar power spectra, and characterisation of the astronomical "seeing" (Roddier 1976). More recently the WSI has been used in ophthalmic research, Licznerski *et al.* (1997) proposed its use in the study of tear-film topography. The tear-film is widely believed to cause a significant amount of variability in wavefront sensing measurements of the eye (Smirnov 1961; Liang & Williams 1997; Hofer *et al.* 2001). This is currently a topic of considerable research interest; reducing the variability of the wavefront sensor measurements would be extremely useful in applications such as refractive eye-surgery. Therefore the shearing interferometer, whose use had declined somewhat over the past 20 years, is still an important wavefront sensing technique and its popularity is increasing once more.

Bates published a paper that said by tilting the mirrors in a Mach-Zehnder Interferometer by a small amount, and thereby producing a lateral shift between the signal and reference beams, fringes would only be observed in the overlap region

(Bates 1947). In the Shearing Interferometer (SI) two copies of the wavefront in the pupil plane are created and one is sheared with respect to the other before placing the interferogram they create onto a 2D detector (see Fig. 7). By operating in the pupil plane the SI is less sensitive to atmospheric noise than traditional speckle interferometers (Roddier & Roddier 1986). There are many different configurations of the SI, which apply the shear a variety of ways the most common being Lateral (LSI), and Rotational (RSI) (Armitage & Lohmann 1965; Ribak 2004). In LSI, when the shear distance is small, the interference will depend on the phase difference between points on the wavefront separated by the shear distance. This phase difference, when normalized with the shear distance, provides a measure of the slope of the wavefront (at that point) in the direction of the shear (Greenaway & Burnett 2004). The wavefront is reconstructed from a pair of interferograms, created by performing the shearing in two orthogonal directions. In this sense it shares something in common with scanning knife edge techniques, covered in Section 8. In RSI, the orthogonal component of the radial shear can be measured by rotating one of the beams by 180° (Tyson 1991). Another variation on the SI is the radial shearing interferometer where copies of the wavefront with different magnifications are combined co-axially to produce an interference pattern over the area of the smaller diameter beam. Radial shear techniques are particularly useful when the wavefront contains only radial aberrations, for example defocus and spherical aberration (Greenaway & Burnett 2004).

WSI, like Shack-Hartmann wavefront sensors, offer fast computation of the wavefront slopes. There are many variations of the shearing interferometer which have been designed to give white-light capability (Wyant 1974), better operation with extended sources (Wyant 1973), increased optical efficiency (Greenaway & Roddier 1980) and phase closure operation (Roddier & Roddier 1986). The WSI remains a versatile wavefront sensing device with applications ranging from Astronomy to Ophthalmology.

6 The Smartt-Point Diffraction Interferometer

The Smartt or Point Diffraction Interferometer (PDI) was popularised by Smartt (Smartt & Strong 1972), but was first described by Linnik (1933). Like WSI, the PDI is a self-referencing interferometer, largely used in optical shop testing of optical elements and lenses (Malacara 1978). The common-path design of the PDI makes it compact and versatile. It is well suited to the testing of large objects, and for use in applications where device size must be kept small, for example in space-borne instruments.

Figure 8 shows how the PDI works in principle. It is well known that a point object will diffract light into a perfectly spherical wave. A plate (marked P in Fig. 8) with a pinhole at its centre is placed into the converging beam from the optical system. The pinhole should be smaller than the size of the Point Spread Function (PSF) of the optical system. This pinhole will thus create a perfect spherical wave, and also allow a portion of the aberrated wavefront to pass through unaltered. The spherical wave and the transmitted part of the wavefront will form
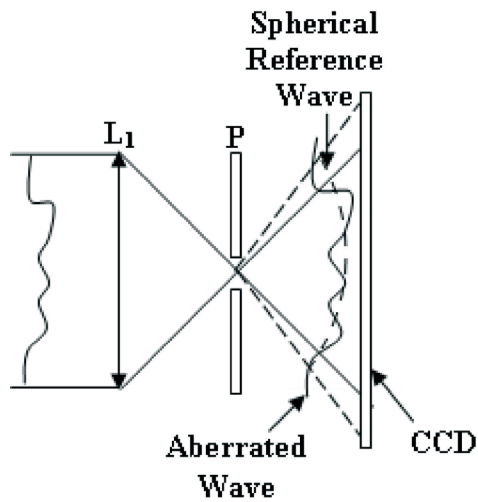
Fig. 8. Schematic of the PDI. A pinhole mask P, placed at the focal plane of lens L_1, creating a spherical reference wave and allowing a small portion of the aberrated wavefront to pass through.

an interference pattern on the camera. It is obvious to see that, due to this design, the PDI is optically very inefficient.

There are a great many variations on the PDI sensor intended to improve its performance in terms of optical efficiency, speed, or convenience of use. An important category of these variations are phase-shifting PDI's. Phase shifting interferometry is the most efficient way of determining the size and direction of wavefront aberration, but the common path design of the PDI makes this a difficult operation to incorporate (Mercer & Creath 1996). It is however possible, Underwood *et al.* (1982) forced the object and reference beams to have different polarizations and created a phase shift using an electro-optic modulator, although this was photometrically very inefficient. Kwon (1984) described a system with a diffraction grating specially designed to produce 3 interferograms simultaneously, which greatly increased the speed of this method, but also required 3 detectors making it expensive and relatively large. Mercer & Creath (1996) demonstrated an interesting phase shifting PDI which uses a liquid crystal layer to introduce the phase shift, with a micro-sphere embedded in its centre to create the spherical reference beam. This device has the advantage of being fully common path and also having easily altered variable phase stepping. Love *et al.* (2005) have also proposed a liquid crystal phase stepping PDI device as a candidate for an Extreme AO (XAO) system, for the imaging of exo-planets and correction of astronomical images from Extremely Large Telescopes (ELTs). Their sensor can be used to give two phase shifted outputs simultaneously, or to drive a phase-only wavefront

corrector. It has the added feature of being capable of giving a null output that can be used to calibrate for scintillation effects.

The advantages of using PDI as a wavefront sensor are that its common-path design makes it robust, lightweight, compact and more stable to vibrations and air turbulence. However, the disadvantages are that it is generally photometrically very inefficient. Also the addition of phase shifting capabilities adds extra optical elements and therefore extra cost, size and weight thus negating some of the benefits of using a common-path device. While this has not been a greatly popular wavefront sensing technique in the past, in comparison to Shack-Hartmann, Phase Diversity and Wavefront Shearing sensors, the PDI is still a useful device. The work of Love *et al.* shows that it is a viable wavefront sensing option for cutting edge applications like XAO (Love *et al.* 2005).

There are some examples of another variation on common-path interferometry that offer attractive wavefront sensing opportunities (Wolfling *et al.* 2004). These authors demonstrated a generalized wavefront analysis system similar in design to the PDI. In this device the pinhole plate is instead replaced by a phase filter containing a "wavefront manipulation function" which acts over a very small area of the input beam. An iterative algorithm is then employed, which uses minimal approximations, to reconstruct the wavefront. They have shown this to be both fast and accurate and it is intended for use in 3D mapping for metrology applications.
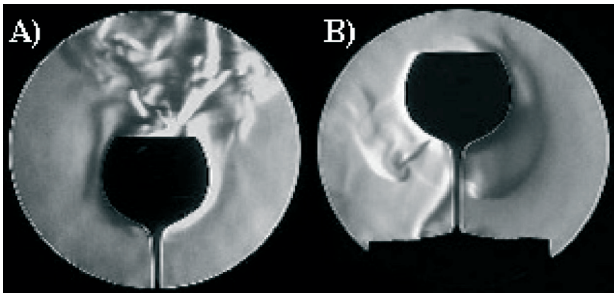
7   Schlieren Imaging

Schlieren imaging, like the Shack-Hartmann, is a technique which involves the division of the input wavefront to gather information about the distortions present in the beam. This technique is a visual process that is used mainly in aeronautical engineering, and for the imaging of turbulent fluid flow (Wikipedia website 2005). This method is mentioned here, as it provides a good introduction for the knife-edge based wavefront sensors which follow.

There are two main ways in which to implement Schlieren imaging; to study fluid flow or to observe distorted wavefronts. In both cases the image that is formed will be scintillated where the subject has gradients or boundaries, or in the case of fluid flow where there are changes in the density of the medium. Figure 9 shows schematically how a Schlieren imaging system works. A distorted wavefront is imaged by a pupil lens and a knife edge is inserted to apodise the focal spot, thus removing certain spatial frequencies from the image. When the truncated image is refocussed onto a CCD camera an image is formed which is bright where the spatial frequencies from the input wavefront were transmitted and dark in regions corresponding to the frequencies blocked by the knife-edge. This variation of the intensity pattern on the camera is essentially a scintillation pattern (GRC 2001). Rainbow Schlieren, (Howes 1984), uses a coloured bull's-eye filter instead of the knife edge which allows the strength of the refraction to be quantified (Wikipedia website 2005; Howes 1984).

In fluid flow applications a collimated beam is used to illuminate the target object (or area). Where the fluid flow is uniform the intensity pattern will be
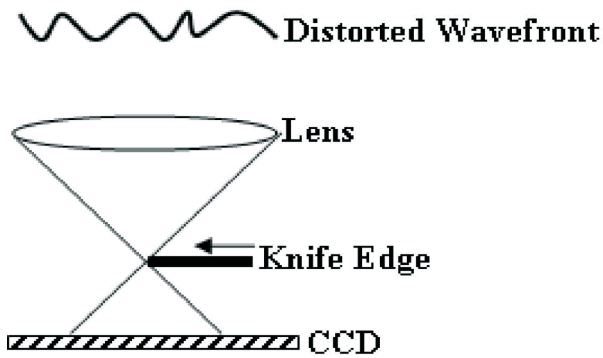
Fig. 9. Schematic demonstrating the basic principle of Schlieren imaging.

Fig. 10. This picture shows Schlieren imaging being used to study convection. The goblet on the left contains boiling water, and that on the right is filled with ice water (used courtesy of Prof. A. Davidhazy, Rochester Institute of Technology 2005).

steady, where there is turbulence a scintillation pattern will be seen. Figure 10 shows a particularly demonstrative example of this. In this example the object is a wine goblet, in one case filled with hot water 10A and in the other, ice water Figure 10B. The Schlieren images in Figure 10 clearly show the air turbulence around the goblet.

The principle advantage of Schlieren imaging is that it is a very low cost system to implement, and has high sensitivity. The main disadvantages of the technique are that the field size under study is limited by the sizes of the optical elements, and that it is only a qualitative visualisation process.

8 Scanning Knife-Edge

The Scanning Knife Edge (SKE) technique is based on the Foucault knife-edge test (Smith 2000) and is similar in principle to the Schlieren imaging method. In SKE, 2D wavefronts are reconstructed from intensity images which are obtained

by scanning 2 knife edges in turn, oriented in orthogonal directions, across the focal plane. As in Schlieren imaging, where the input wave is aberrated, the knife edge will block light entering the pupil plane where the local slope is greater than the value determined by the position of the knife edge. Combining the data from the scans of the two knife edges allows the wavefront in the pupil plane to be reconstructed from the local slope measurements (Greenaway & Burnett 2004).

Disadvantages of this technique are that diffraction at the knife edge causes blurring in the images that making difficult to distinguish exactly where boundaries lie, and also that the scanning process takes a significant length of time to complete (Greenaway & Burnett 2004). The latter is by far the most limiting drawback, as it means this method is unsuitable for situations in which the aberrations are dynamic and rapidly changing, for example in ophthalmic applications.

9   Pyramid or Scanning Prism Knife Edge

The Pyramid Wavefront Sensor (PWS) was proposed as a new sensor for astronomical applications intended to become a rival of the Shack-Hartmann and Curvature sensors usually used in this field (Ragazzoni 1996). The principle behind the operation of the Pyramid sensor is similar to the SKE, and also to the sensor described by Horowitz (1978) and the concepts illustrated by Sprague & Thompson (1972). Sprague and Thompson demonstrated an early coherent imaging system design which produced an image whose irradiance was directly proportional to the wavefront phase for large phase variations. This was an interesting technique, but involved a time consuming photographic step to create a filter and was therefore not suitable for real-time applications. Horowitz further developed this idea, and instead employed a specially designed filter (in place of the photographic filter) to create an output intensity image which is linear with the derivative (*i.e.* slope) of the phase function. In the pyramid sensor proposed by Ragazzoni a pyramid is used to fulfil the same role as the filters described by Horowitz, Sprague and Thompson, and this new wavefront sensor also shares characteristics with the modulation contrast microscope (Hoffman & Gross 1975). It is an interesting and relatively new type of wavefront sensor which is increasingly popular amongst researchers, but still not as widely used as the Shack-Hartmann or Curvature sensors.

Figure 11 shows the basic configuration of the PWS. A prism, or pyramid, is placed in the focal plane of the lens L_1 (which may be the exit pupil of a telescope for example) so that the incoming light is focussed onto the vertex of the pyramid. The four faces of the pyramid will deflect the portion of the beam incident on them in slightly different directions. The lens relay, simplified and called L_2 in Figure 11, is used to conjugate the optical system exit pupil with the focal plane of L_2 where the CCD camera is situated. At the CCD 4 images, one from each face, are seen. The sensor is based on the same quad-cell arrangement as the Shack-Hartmann sensor (Fig. 1). If the system is un-aberrated and the effects of diffraction are ignored, then the 4 pupil images should be identical (Iglesias *et al.* 2002). It was mentioned above that the pyramid sensor is similar to the SKE technique, the reason being that by taking the sum of images $a + b$, one exactly obtains the
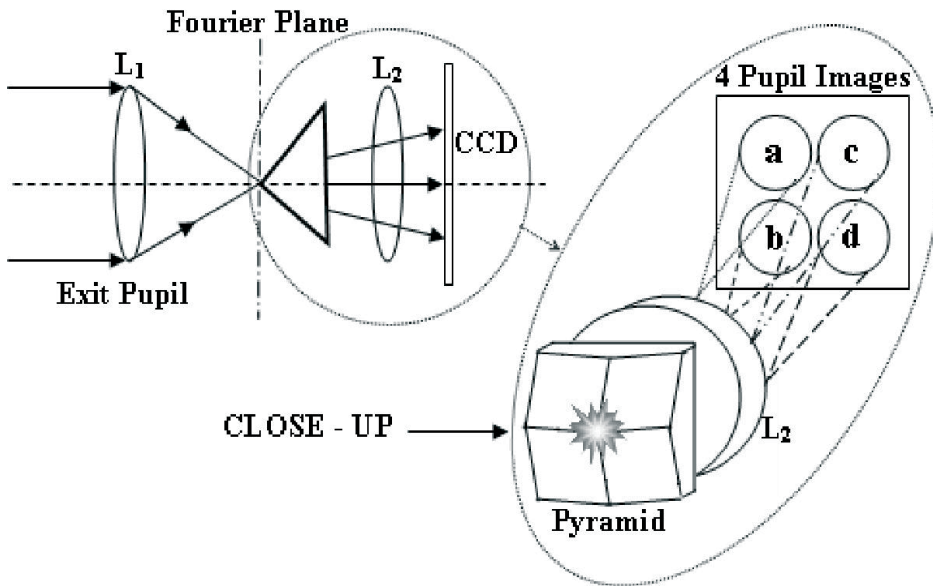
Fig. 11. The Pyramid Wavefront Sensor.

image that would be obtained by a knife edge test. The data required from the orthogonal direction is found by adding $c + d$. In this way the PWS overcomes the main disadvantage of the SKE, as the data is obtained simultaneously and not by scanning the knife edges and it also has better optical efficiency.

Problems occur if the wavefront slope is so large that all of the incoming light is incident on only one facet of the pyramid. In this situation the signal received is independent of the gradient modulus and the detector quad cell assigned to that facet will be saturated (Iglesias *et al.* 2002). To avoid this problem Ragazzoni proposed that the pyramid (or the input field) should be oscillated (Ragazzoni 1996; Iglesias *et al.* 2002).

The advantages of the PWS are that the sampling and the gain of the instrument are easily adjustable. The sampling, which is the size of the pupil on the detector, can be dynamically adjusted by using a zoom lens arrangement for the relay L_2 (see Fig. 11), and the gain can be altered by changing the vibration amplitude of the prism (Ragazzoni 1996). This means that with this sensor it would be possible to perform wavefront sensing on sources of varying brightness and different degrees of aberration (Greenaway & Burnett 2004). This is important in ophthalmic applications where the eye aberrations of different patients can vary by large amounts. This sensor has been shown to work very well (to estimate the aberrations of the eye) with the human eye as an extended source (Iglesias *et al.* 2002). This sensor has also been developed for astronomical applications such as

the phasing of large telescope mirrors (Gonte *et al.* 2005) and for Multi-Conjugate AO, where multiple pyramids are used to characterise more than one turbulent atmospheric layer at a time (Diolaiti *et al.* 2002).

10 The Modal Wavefront Sensor

The modal sensor proposed by Neil *et al.* (Neil *et al.* 2000) is the final wavefront sensor which we will considered in this article. As a modal sensor it does not measure the slope or curvature of the wavefront, but instead directly measures the size of any chosen Zernike mode present in the wavefront (Neil *et al.* 2000). This is a very interesting wavefront sensor, with similarities to the diffraction grating based phase diversity sensors discussed earlier in Section 3.

In this modal sensor a diffraction grating is used to produce pairs of spots for each orthogonal mode to be measured. In each spot pair, one image is formed by adding a positive bias and the other by adding a negative bias to the input beam. The pairs of beams are focussed down, and passed through an aperture mask, onto a detector. When the input wavefront is plane there are no offsets in the beams, they all pass through the aperture mask so that the optical power in each of the spots will be the same. When aberrations are present in the beam the intensity in the spot pairs will vary according to which modes are present, as the beam offsets will affect how much light is passed through the aperture mask.

The modal sensor is of particular use in applications such as confocal microscopy, where the number of aberration modes is relatively few (compared to atmospheric turbulence for example). In this case the modal sensor saves time and effort by not performing a full wavefront reconstruction and instead can be limited to study only the aberrations of greatest interest.

11 Image Sharpening and Indirect Methods

Indirect wavefront sensing techniques, instead of calculating the wavefront aberration and then applying a correction, seek to apply correction until some chosen error metric has been minimised. This error metric can be any real-time varying quantity that is affected by wavefront aberration. The most common choice is intensity at focus, but image sharpness and scattered field statistical moments are also used (Muller & Buffington 1974; Hardy 1978; Tyson 1991; Vorontsov *et al.* 1996; Polejaev & Vorontsov 1997; Cohen & Cauwenberghs 2002).

Image Sharpening (IS), is an algorithm as opposed to an actual sensor. Historically this technique originates from the first astronomy applications of taking atmospherically degraded images and turning them into sharp images. In its most basic configuration IS works by moving a single phase adjuster at a time and observing the integrated intensity squared in the image plane. Using Parseval's Theorem it is easy to show that this metric (also known as the image sharpness) is maximised when the wavefront is flat. When the maximimum is found the phase adjuster is left at this position, another actuator is chosen, and the image is studied in the same way. This can be a time consuming process and uses very little
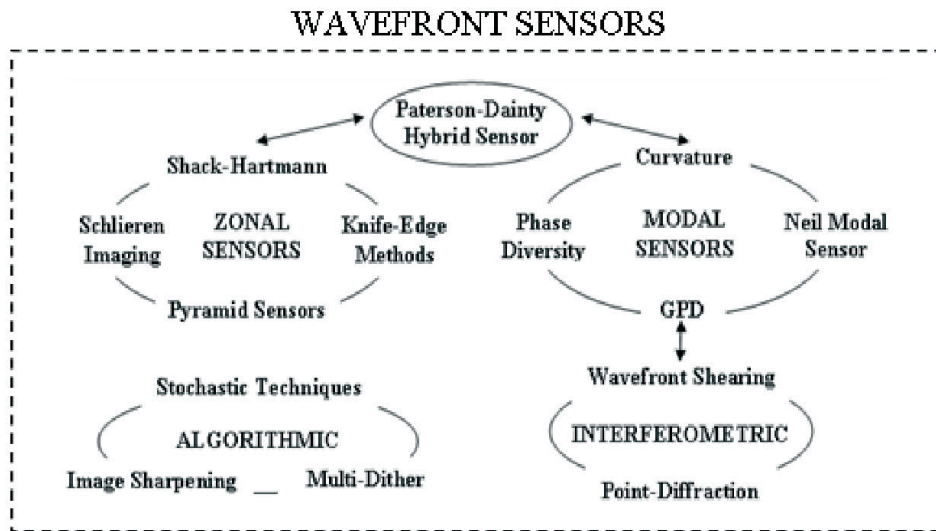
WAVEFRONT SENSORS

Fig. 12. Diagram summarising the Wavefront Sensing techniques discussed in this article. Arrows illustrate links between specific wavefront sensors.

of the image information available. This technique is also only effective on bright point-like objects close to the optic axis, which is why it's used by astronomers for bright stars, but is of limited use elsewhere.

This technique is similar to the multi-dither approach (Youbin *et al.* 1998), which, instead of referring to a single phase adjuster, considers the wavefront as a whole. The corrective element is moved and the change to the image sharpness is assessed. If the image sharpness has increased then the change is accepted and the corrective element is moved a little further in the same direction. If however the change is detrimental then the corrective element is moved back and in the opposite direction. This process is repeated until the wavefront has been flattened. The advantage of this technique is that all of the available light is used, but the disadvantage is that it can be time consuming to arrive at the optimal solution for the corrective element position.

Other indirect methods can include stochastic techniques, which are statistical methods for the effective minimisation of the chosen error metric. These techniques are often formulated to be "model-free" which means that they are independent of the complexity of the optical system used and do not require any *a priori* information about the function under test (Cohen & Cauwenberghs 2002).

Since direct measurement of the wavefront phase can be computationally very expensive, in indirect methods the burden is shifted to the accurate measurement of the chosen quality metric. In applications like astronomy, where one simply seeks to remove the aberrations on the input field, these methods can give faster results than performing a full wavefront reconstruction. In metrology however,

where the shape of the wavefront may represent the shape of some test surface, reconstruction is necessary and these methods are of limited use.

12   Conclusions

Figure 12 summarises the techniques which have been discussed in this article and shows how the different wavefront sensing techniques are interrelated. Arrows are used to link specific wavefront sensors, whereas lines are used to group the sensors into categories that share common properties.

This paper has shown that wavefront sensing is a diverse field, and has provided a basic introduction to what the authors believe to be the most historically and currently important classes of wavefront sensor types.

References

Armitage, & Lohmann, 1965, Opt. Acta, 12

Babcock, H.W., 1953, PASP, 65(386), 229

Barakat, R., & Newsam G., 1984, J. Math. Phys., 25(11), 3190

Barty, A., Nugent, K.A., *et al.*, 1998, Opt. Lett., 23(11), 817

Bates, W.J., 1947, Proc. Roy. Soc., 59, 940

Blanchard, P.M., & Greenaway, A.H., 1999, Appl. Opt., 38(32), 6692

Blanchard, P.M., Fisher, D.J., *et al.*, 2000, Appl. Opt., 39(35), 6649

Blanchard, P.M., & Greenaway A.H., 2000a, Opt. Comm., 183(1–4), 29

Blanchard, P.M., & Greenaway A.H., 2000b, Trends in Optics and Photonics. Diffractive Optics and Micro-Optics, 41, Technical Digest, Postconference Edition, Opt. Soc. America

Burge, R.E., Fiddy, M.A., *et al.*, 1976, Proc. Roy. Soc. A, 350, 191

Campbell, H.I., Zhang, S., *et al.*, 2004a, Opt. Lett., 29(23), 2707

Campbell, H.I., Zhang, S., *et al.*, 2004b, AMOS Technical Conference, Published on CD, contact `amostech@maui.com`

Campbell, H.I., Zhang, S., *et al.*, 2005, The 5th International Workshop on Adaptive Optics in Industry and Medicine, Proc. SPIE, 6018, to be published

Carmody, M., Marks, L.D., *et al.*, 2002, Physica C, 370, 228

Cohen, D.K., Gee, W.H., *et al.*, 1984, Appl. Opt., 23(4), 565

Cohen, M., & Cauwenberghs, G. 2002, IEEE Sensors J., 2(6), 680

Dainty, J.C., & Fiddy, M.A. 1984, J. Mod. Opt., 31(3), 325

Davidhazy, A., accessed 16/06/05 `http://www.rit.edu/~andpph/text-schlieren.html`

Diolaiti, E., Tozzi, A., *et al.*, 2002, Proc. SPIE, 4839, 299

Dolne, J.J., & Schall, H.B. 2004, AMOS Technical Conference, Published on CD, contact `amostech@maui.com`

Dreher, A.W., Bille, J.F., *et al.*, 1989, Appl. Opt., 28(4), 804

ESO, 2003, `http://aanda.u-strasbg.fr:2002/articles/aa/full/2003/07/aa2912/node2.html`, accessed 31/10/2003

Gerchberg, R.W., & Saxton, W.O. 1972, Optik (Stuttgart), 35, 237

Give'on, A., Kasdin, N.J., *et al.*, 2003, Proc. SPIE, 5169, 276

Gonsalves, R.A., 1982, Opt. Eng., 21(5), 829

Gonsalves, R.A., 1987a, Proc. SPIE, 351, 56

Gonsalves, R.A., 1987b, J. Opt. Soc. Am. A, 4(1), 166

Gonte, F., Yaitskova, N., *et al.*, 2005, Proc. SPIE, 5894, 306

GRC, 2001, `http://www.grc.nasa.gov/WWW/OptInstr/schl.html`, accessed 16/06/05

Greenaway, A., & Roddier, C., 1980, Opt. Comm., 32(1), 48

Greenaway, A.H., Campbell, H.I., *et al.*, 2003, 4th International Workshop on Adaptive Optics in Industry and Medicine (Springer) Proc. Phys., 102

Greenaway, A., & Burnett, J., 2004, Technology Tracking: Industrial and Medical Applications of Adaptive Optics (London, IOP Publishing Ltd.)

Gureyev, T.E., Roberts, A., *et al.*, 1995, J. Opt. Soc. Am. A, (9), 1932

Gureyev, T.E., & Nugent, K.A., 1996, J. Opt. Soc. Am. A, 13(8), 1670

Hardy, J.W., 1978, Proc. IEEE, 66, 651

Hofer, H., Artal, P., *et al.*, 2001, J. Opt. Soc. Am. A, 18(3), 497

Hofer, H., Chen, L., *et al.*, 2001, Opt. Ex., 8(11), 631

Hoffman, R., & Gross, L., 1975, Appl. Opt., 14, 1169

Horwitz, B.A., 1978, Appl. Opt., 17(2), 181

Howes, W.L., 1984, Appl. Opt., 23, 2449

Iglesias, I., Ragazzoni, R., *et al.*, 2002, Opt. Ex., 10(9), 419

Jefferies, S.M., Lloyd-Hart, M., *et al.*, 2002, Appl. Opt., 41(11), 2095

Kendrick, R.L., Acton, D.S., *et al.*, 1994, Appl. Opt., 33(27), 6533

Kudryashov, A., Samarkin, V., *et al.*, 2003, 4th International Workshop on Adaptive Optics in Industry and Medicine (Springer) Proc. Phys., 102

Kwon, O.Y., 1984, Opt. Lett., 9, 59

Levecq, X., 2005, Opto and Laser Europe, Sep. 2005 issue

Liang, J., Grimm, B., *et al.*, 1994, J. Opt. Soc. Am. A, 11(7), 1949

Liang, J., & Williams, D.R., 1997, J. Opt. Soc. Am. A, 14(11), 2873

Licznerski, T.J., Kasprzak, H.T., *et al.*, 1997, 10th Slovak-Czsch-Polish Optical Conference on Wave and Quantum Aspects of Contemporary Optics, Int. Soc. Opt. Eng., 3320, 183

Linnik, V.P., 1933, C.R. Acad Sci. USSR, 1, 208

Love, G., Oag, T.J.D., *et al.*, 2005, Opt. Ex., 13(9), 3491

Malacara, D., 1978, Optical Shop Testing (New York, Wiley)

Mercer, C.R., & Creath, K., 1996, Appl. Opt., 35(10), 1633

Muller, R.A., & Buffington, A. 1974, J. Opt. Soc. Am. A, 64(9), 1200

Neil, M.A.A., Booth, M.J., *et al.*, 2000, J. Opt. Soc. Am. A, 17(6), 1098

Nieto-Vesperinas, M., Navarro, R., *et al.*, 1988, J. Opt. Soc. Am. A, 5(1), 30

Noll, R.J., 1976, J. Opt. Soc. Am. A, 66, 207

Paterson, C., & Dainty, J.C., 2000, Opt. Lett., 25(23), 1687

Platt, B.C., & R. Shack, 2001, J. Refractive Surgery, 17 (Sep./Oct.)

Polejaev, V.I., & Vorontsov, M.A., 1997, Proc. SPIE, 3126

Quiroga, J.A., Gomez-Pedrero, J.A., *et al.*, 2001, Opt. Eng., 40(12), 2885

Ragazzoni, R., 1996, J. Mod. Opt., 43(2), 289

Rao, C.H., Jiang, W.-H., *et al.*, 2002, Chin. Astron., 26(1), 115

Ribak, E., 2004, Proc. SPIE, 5491, 1194

Robinson, S.R., 1978, J. Opt. Soc. Am. A, 68, 87

Roddier, C., 1976, J. Opt. Soc. Am. A, 66(5), 478

Roddier, F., & Roddier, C., 1986, Opt. Comm., 60(6), 350

Roddier, F., 1988, Appl. Opt., 27(7), 1223

Rousset, G., Bauzit, J.L., *et al.*, 1993, ESO Conf. and Workshops Proc., 48, 65

Schiske, P., 1975, J. Phys. D, 8, 1372

Shahidi, M., Blair, N.P., *et al.*, 2004, Optom. Vis. Sci., 81(10), 778

Smartt, R.N., & Strong, J., 1972, J. Opt. Soc. Am. A, 62, 737

Smirnov, H.S., 1961, Biophys., 6, 52

Smith, M.W., 2004, Proc. SPIE, 5524

Smith, M.W., & Wick, D.V., 2004, AMOS Technical Conference, Published on CD,
    contact `amostech@maui.com` or visit `www.maui.afmc.af.mil` for a copy

Smith, W. J., 2000, Modern Optical Engineering, SPIE Press

Sprague, R.A., & Thompson, B.J., 1972, Appl. Opt., 11(7), 1469

Teague, M.R., 1982, J. Opt. Soc. Am. A, 72(9), 1199

Teague, M.R., 1983, J. Opt. Soc. Am. A, 73(11), 1434

Thust, A., Lentzen, M., *et al.*, 1997, Scann. Microsc., 11, 437

Tyson, R.K., 1991, Principles of Adaptive Optics (London, Academic Press Ltd.)

Underwood, K., Wyant, J.C., *et al.*, 1982, Proc. SPIE, 351, 108

Van Dam, M.A., & Lane, R.G., 2002, J. Opt. Soc. Am. A, 19(7), 1390

Van Dam, M.A., & Lane, R.G., 2002, Opt. Eng., 41(6), 1387

Vorontsov, M.A., Carhart, G.W., *et al.*, 1996, J. Opt. Soc. Am. A, 13(7), 1456

Welch, S., Greenaway, A., *et al.*, 2003, Astron. Geophys., 26-9

Wikipedia, online encyclopedia, accessed 16/06/05,
    `http://en.wikipedia.org/wiki/Schlieren_photography`

Williams, D.R., 2005, accessed 18/10/05,
    `http://www.cvs.rochester.edu/williamslab/r_shackhartmann.html`

Wolfling, S., Ben-Yosef, N., *et al.*, 2004, Opt. Lett., 29(5), 462

Woods, S.C., & Greenaway, A.H., 2003, J. Opt. Soc. Am. A, 20(3), 508

Wyant, J.C., 1973, Appl. Opt., 12, 2057

Wyant, J.C., 1974, Appl. Opt., 13, 200

Youbin, F., Xuerning, Z., *et al.*, 1998, Opt. Eng., 37(4), 1208

Zhang, S., Campbell, H.I., *et al.*, 2003, 4th International Workshop on Adaptive Optics
    in Industry and Medicine, Springer Proceedings in Physics, 102

Zhang, S., Campbell, H.I., *et al.*, 2005, The 5th International Workshop on Adaptive
    Optics in Industry and Medicine, SPIE Proceedings, 6018, to be published